Analyst

PAPER

View Article Online
View Journal | View Issue

Cite this: *Analyst*, 2026, **151**, 2533

Utilizing Venturi effect for automated high-throughput droplet-MS from well plates

Bridget E. Murray, [a] Roger C. Diehl, [b] Moritz Pott,[c] Daniel A. Holland-Moritz, [d] Alison R. H. Narayan [a,b] and Robert T. Kennedy *[a,e]

High-throughput screening is important in a diverse array of applications including drug discovery, synthetic reaction development, and enzyme engineering. Well plates are often used for sample preparation and containment in such applications, so analytical methods that are compatible with this format are required. Mass spectrometry (MS) is an attractive analytical technique for high-throughput analysis due to its potential for rapid, sensitive, selective, and label-free multiplexed measurements. Here, we present a method that uses the Venturi effect to withdraw droplet samples from a well plate and infuse them to the electrospray ionization (ESI) source of a mass spectrometer. The Venturi effect is generated by flow of nebulizing gas through a constriction at the outlet of the ESI source. The resulting negative pressure allows sample to be pulled to the ESI source *via* a sample transfer capillary that is coaxial with the ESI source at the outlet and can be dipped into sample at the inlet. To keep different samples from mixing, 380 nL sample plugs flowing at 330 μL min^{-1} are sipped into the source and separated by air gaps resulting in segmented flow to the source. The system requires no valves or connections for achieving sample pick-up and analysis. An *x*,*y*,*z*-positioner is used to move the sample inlet for automated sampling from different wells. Increasing capillary inner diameter and nebulizing gas pressure increased the throughput of Venturi droplet-MS by increasing sample flow rate. An interaction of sample plug size and number within the capillary on overall flow rate was observed and affected the possible throughput. When using perfluoroalkoxy alkane (PFA) tubing as the transfer capillary, carryover between samples was 0.88 ± 0.16%. The method is demonstrated by screening 283 whole cell reactions for enzyme engineering at 0.4 samples per s, while showing good agreement (R^2 = 0.92) with liquid chromatography-mass spectrometry (LC-MS). This work improves upon previous uses of segmented flow for high-throughput MS by integrating sample generation and transfer in one step. Compared to other high-throughput MS methods this approach requires no custom MS sources or specialty sample introduction equipment.

Received 21st January 2026,
Accepted 4th March 2026

DOI: 10.1039/d6an00065g

rsc.li/analyst

1. Introduction

High-throughput screening is important in a diverse array of endeavors including diagnostics, drug discovery, organic reaction development, hybridoma selection, and enzyme engineering.[1–12] UV-vis- and fluorescence-based assays have commonly been employed for such screening due to their potential for high analysis rate,[13–15] but mass spectrometry (MS) has gained importance in high-throughput applications because of its capability for selective, multiplexed, and label-free analysis.[16,17] Droplet microfluidics offers one way to combine high-throughput sample manipulation with MS;[18–20] however, the majority of high-throughput experiments are performed using multi-well plates for sample containment.[21–23] Therefore, methods that can transfer samples rapidly from well plates to a mass spectrometer are needed. In this work, we explore using the Venturi effect to create and transfer sample plugs (droplets) segmented by air from a well plate to an electrospray ionization (ESI) source for MS analysis.

A variety of high-throughput (*i.e.*, 1–15 s per sample) MS methods have been developed that interface with well plates including fast solid phase extraction-mass spectrometry (SPE-MS),[24–27] acoustic mist ionization-mass spectrometry (AMI-MS),[28–30] and open port interface-mass spectrometry (OPI-MS)[31]/acoustic droplet ejection-open port interface-mass spectrometry (ADE-OPI-MS).[32–35] In these examples, sample transfer to the mass spectrometer is achieved by use of external pumps (SPE-MS), acoustic ejection (AMI-MS), or the

[a]*Department of Chemistry, University of Michigan, Ann Arbor, MI 48109, USA. E-mail: rtkenn@umich.edu*
[b]*Life Sciences Institute, University of Michigan, Ann Arbor, MI 48109, USA*
[c]*BASF SE, 67056 Ludwigshafen am Rhein, Germany*
[d]*Process Research and Development, Merck & Co., Inc., Rahway, New Jersey 07065, USA*
[e]*Department of Pharmacology, University of Michigan, Ann Arbor, MI 48109, USA*

Venturi effect created by a custom open port interface (OPI-MS/ADE-OPI-MS). These methods provide meaningful advancements in high-throughput screening, but further improvements remain of interest due to their requirements for specialty equipment and high introductory costs.

Sample transfer *via* self-aspiration (*i.e.*, flow not driven by external pumps or valves) is an alternative strategy with potential for low cost. Examples include flow driven by capillary action,[36] by the vacuum created by the mass spectrometer source,[37] and by the Venturi effect created in the mass spectrometer source. The capillary action approach is low-cost but not easily adaptable to rapid, multi-sample analysis. Leveraging the vacuum created by a mass spectrometer is easily adaptable to multi-sample analysis but requires custom instrumentation for analysis of liquid samples while providing moderate throughput of 0.1 samples per s. However, the Venturi effect created by the mass spectrometer source can provide high-throughput analysis of multiple samples without custom instrumentation or high introductory costs.

Previous work has shown the feasibility of coupling well plates to MS with Venturi-Easy ambient sonic-spray ionization (V-EASI).[38] In this approach, the Venturi effect, caused by constriction of a flowing fluid, is created at the exit of a transfer tube that interfaces to the mass spectrometer.[38] The resulting pressure differential allows samples to be aspirated from the well plate to the sonic spray ionization source,[32] enabling automated sample generation and infusion from a well plate. This initial study used a custom-built MS source to aspirate 150 nL samples segmented by air.[38] The use of segmented flow allows for high-throughput introduction of discrete samples without dilution from a miscible carrier phase. The method was demonstrated on 30 purified enzyme samples for interrogation of inhibitor potency at a throughput of 0.6 samples per s.[38] This strategy has the advantage of requiring minimal sample introduction equipment. It also automates the transition from well plate to droplet to detection, which has been an issue in well-plate based droplet-MS.[10,39–41] Relatedly, robotically automated vacuum enabled direct-inject mass spectrometry (RAVE MS) utilized a commercially available sheath flow MS source and single quadrupole mass spectrometer for analyzing bio- and chemo-catalytic reactions at 0.1 samples per s.[42]

Here, we use a commercially available ESI-MS source to generate and infuse sample droplets segmented by air using the Venturi effect. The system is simple to implement as no user intervention, unions, valves, or connections besides a single piece of tubing are needed to generate and transfer droplets to the mass spectrometer for detection. This work expands upon V-EASI (0.6 samples per s),[38] OPI-MS (0.5[35] to 3[31,32] samples per s),[31,32,35] and RAVE MS work (0.1 samples per s)[42] by demonstrating similar or higher throughput without specialty equipment. We also address remaining challenges in application of the Venturi effect to high-throughput droplet-MS, including limits on throughput, methods of controlling flow, and carryover. Key operation parameters that affect throughput (*e.g.*, nebulizing pressure, capillary inner diameter, and droplet size) are described, and their quantitative effect on droplet flow rate is evaluated. Carryover is evaluated in different droplet transfer line materials. The system is demonstrated by screening 283 whole cell hydantoinase reactions producing butyl glufosinate created for a directed evolution campaign at 0.4 samples per s, illustrating the potential for high-throughput screening by direct-MS using this method.

2. Materials and methods

2.1. Chemicals and reagents

All chemicals were purchased from Sigma-Aldrich (Saint Louis, MO) unless otherwise noted. The butyl glufosinate standard was prepared *via* an enzymatic cascade outlined below.

2.2. Directed evolution and enzymatic cascade

Using a homology model of a hydantoinase from *Frigidibacter mobilis* (GenBank accession number WP_066814531), 96 residues were selected for site-directed mutagenesis (SDM). Single mutations were made *via* PCR using a pair of primers with a randomized codon, and DH5α *E. coli* were transformed with the ligated PCR product. After validation of successful mutagenesis by Sanger sequencing, TG10+ expression strain *E. coli* cells were transformed with the resulting library. In later rounds, top mutations from the previous round were used for combinatorial SDM to identify synergies between beneficial mutations, and TG10+ cells were transformed with these libraries as well. Colonies of this expression strain were then grown in 96-well plates, alongside template (*i.e.*, starting enzyme that engineering was performed on) and inactive enzyme controls using variants that previously demonstrated no activity towards the substrate.

Variants were evaluated in a two-enzyme sequence with 2.5 mM racemic hydantoin butyl glufosinate as a substrate. The hydantoin is converted to D- and L-carbamoylic acid by the hydantoinase, and the L-carbamoylic acid is then converted to the final L-glufosinate product by an L-selective carbamoylase. The initial hydantoinase was from *Frigidibacter mobilis*.[43] Variant hydantoinase and NCS 1–23 carbamoylase (Uniprot A0A535Y1H2) were produced in whole *E. coli*, with each enzyme in a different strain under a rhamnose induction system in a pDHE plasmid. Reactions were carried out in sealed plates in 100 mM HEPES buffer with 100 mM NaCl and 1 mM $MnCl_2$. As NCS 1–23 cannot hydrolyze butyl D-glufosinate carbamoylic acid, the ratio of glufosinate to total product as measured by mass spectrometry was used as a proxy for L-selectivity of the hydantoinase.

2.3. Liquid chromatography-mass spectrometry analysis of enzymatic cascade reactions

After 24 h, samples were diluted four-fold to a final solvent concentration of 20/80 methanol (MeOH)/water containing 0.1% formic acid. Sample plates were centrifuged for 10 min at 1000*g* to pellet cells, then aliquots from each well were diluted 10-fold in 20/80 MeOH/water containing 0.1% formic

acid and filtered through centrifugal filter plates. Samples were analyzed by LC-MS on an Agilent 6230 LC-TOF system with a Phenomenex Kinetex 100 × 2.1 mm C18 column with a 1.7 μm particle size and a 100 Å pore size using a 3 minutes separation method at 0.2 mL min^{-1} and 40 °C with an isocratic eluent of 20% B. Mobile phase A was 95/5 water/acetonitrile containing 0.1% formic acid and mobile phase B was 5/95 water/acetonitrile containing 0.1% formic acid. The $M + H^+$ ion was detected using a 140 V fragmentor voltage and used for quantification. An example chromatogram is shown in Fig. S1.

The variants with the highest L-selectivity of each round as determined by LC-MS were then streaked on new plates from glycerol stocks and used in a validation assay along template controls. These reactions were analyzed both by achiral LC-MS as above and by chiral LC-MS with an Astec Chirobiotic-T2 250 × 4.6 mm teicoplanin column with 5 μm particle size to differentiate the L- and D-enantiomers of butyl glufosinate and carbamoylic acid. Chiral LC-MS used the same instrument and detection parameters as above, but the mobile phase flow rate was 0.7 mL min^{-1}, column temperature was 25 °C, and a 16 min gradient of 90% B to 65% B was used, with mobile phases A and B being the same as above, followed by a 1 min gradient back to 90% B and a 5 min re-equilibration at 90% B.

2.4. LC-MS data analysis

The butyl glufosinate peak area was normalized to all analyte (butyl glufosinate, carbamoylic acid, and hydantoin) peak areas to help ensure results were reliable (*i.e.*, so that potential differences in injection volume were accounted for[44]). Relative quantification was performed by dividing the normalized butyl glufosinate peak area in an enzyme variant sample by the average normalized butyl glufosinate peak area from biological replicates ($n = 7$) of template enzyme reactions. All calculations were performed in Excel.

2.5. Sample preparation for Venturi droplet-MS/MS analysis

Quenched enzymatic reactions were stored in 96-well plates covered with an adhesive foil seal at −80 °C until needed. Thawed enzymatic reaction mixtures were diluted 15-fold by adding 6.9 μL of sample to 97 μL of dilution solvent, which was composed of 20/80 MeOH/18 MΩ water containing 0.1% formic acid (v/v) and 2.7 μM acetylcholine, in a 96-well plate. The diluted enzymatic reaction mixtures were mixed by pipetting up and down three times with a P100 multichannel pipette set to 50 μL.

20 μL of diluted enzymatic reaction mixture was transferred from the 96-well plate to a Grenier 384-well plate (Monroe, NC) for droplet generation. The contents of only one 96-well plate were placed in a 384-well plate at a time, so droplets were created from a 384-well plate but only a 96-well plate was screened at a given instance. Each well plate contained a set of calibration standards covering the following concentrations: 0.0, 0.7, 1.3, 2.0, 2.7, and 3.3 μM (concentration after 15-fold dilution) butyl glufosinate. Marker droplets, which were composed of 2.7 μM acetylcholine in 20/80 MeOH/18 MΩ water containing 0.1% formic acid (v/v), were inserted into the train of sample and calibration droplets to help ensure sample registry with wells.

2.6. Venturi droplet-MS/MS

Air-segmented droplets were formed by alternately dipping the inlet end of 150 μm inner diameter (i.d.) × 360 μm outer diameter (o.d.) × 70 cm long perfluoroalkoxy alkane (PFA) tubing from Idex (Lake Forest, IL) between solution in wells and ambient air with the outlet end of tubing threaded through an Agilent capillary electrophoresis-mass spectrometry (CE-MS) source for enzyme reaction screening. 150, 200, and 250 μm i.d. × 360 μm o.d. × 70 cm long fused silica capillary was also tested for droplet generation and infusion. Solution is aspirated when the tubing is dipped into a solution and the source MS nebulizing gas is at a sufficient pressure. Unless otherwise noted, the nebulizing gas pressure was set to 60 psi. The tubing was moved across a well plate using an *x*,*y*,*z*-computer numerical control (CNC) machine operated by G-code. To create droplets, the tubing inlet was lowered 7 mm into the well and held there for 0 s before returning to 1.5 mm above the well (zero position) in air where it is held for 2 s, unless otherwise noted. All wells were sampled in triplicate. When analyzing a sequence of droplets, three wells were sampled in triplicate before and after the start of calibration standard and sample infusion to keep flow rate stable during analysis. PFA tubing was positioned so that it was approximately 0.1 mm beyond the end of the MS source. Tubing was consistently placed in the same approximate location (by eye) based on where stable spray of the droplets is achieved. A sheath liquid (20/80 MeOH/18 MΩ water containing 0.1% formic acid (v/v)) was delivered at 0.1 mL min^{-1} by an Agilent 1290 binary pump and flowed coaxially with nebulizing gas and droplets through the CE-MS source.

Droplets were analyzed using an Agilent 6410 QQQ operated in multiple reaction monitoring (MRM) mode acquiring the following analyte fragmentation pairs: 238.2 → 136 for butyl glufosinate and 146.1 → 87.1 for acetylcholine. The fragmentor voltage was 75 V for butyl glufosinate and 70 V for acetylcholine. For both analytes, dwell time was 0.5 ms, collision energy was 13 V, and MS1 and MS2 were operated at unit resolution. MS source settings were: capillary voltage = 3500 V, drying gas flow rate = 10 L min^{-1}, nebulizing pressure = 60 psi, drying gas temperature = 350 °C, unless otherwise noted.

2.7. Droplet-MS data analysis

Analyte specific MRM traces were used for relative quantification. The MRM traces were examined in the Agilent Qualitative Navigator software, exported into a .csv or .xls file, and then analyzed in Excel. Droplet signal was separated from baseline by using an Excel IF function to copy the ion intensity value to a new column if the acetylcholine ion intensity was above a user-set threshold. These values were then averaged using a combination of COUNT, AND, and AVERAGE functions in Excel. The averaged droplet signal was used for further analysis. Since each well was sampled in technical triplicate, this

droplet average was then averaged with the other two replicate droplet averages from a given well to yield the butyl glufosinate signal that was used for relative quantification. The averaged value of n = 3 droplets was then divided by the butyl glufosinate droplet signal from the average of n = 7 biological replicates (each biological replicate was also sampled in technical triplicate for droplet analysis) of the template enzymatic reaction, yielding the fold-improvement of an enzyme variant relative to the template enzymatic reaction.

2.8. Volume, flow rate, and throughput analysis

Droplet volume and flow rate were measured at approximately the halfway point between the tubing inlet (at the well plate) and outlet (in the MS source) using recorded videos and ImageJ. If flow stopped prior to this point, droplet volumes were measured after the generation process using a ruler and microscope. Flow rate was calculated by dividing the volume traversed by the leading edge of a droplet over ~6 cm of length (exact length depended on the specific droplet flow rate being measured) and dividing this value by the time it took the droplet to traverse that length. For flow rate measurements where only a single droplet was present in the tubing at a time, flow rate was calculated as the volume of the entire transfer tubing divided by the time it took the droplet to traverse that volume. Aqueous and air segments were assumed to have a cylindrical shape for volume calculations. The cylindrical shape was verified under a microscope. Dimensionless droplet lengths were calculated as droplet length divided by radius, given by radius of the droplet tubing.

To determine the droplet volume and flow rate for the screening experiment, n = 6 droplets were measured at three evenly spaced intervals over the course of 10 minutes for a total of 18 measurements. Air spacing was not measured as it was larger than the camera frame used to measure droplet volume and flow rate.

Throughput of a 96-well plate was calculated by counting the number of droplets detected by MS in a 0.2 min period. This value was averaged with the throughput observed for two other 96-well plates yielding an average of 0.4 samples per s.

2.9. Droplet carryover

Droplet carryover was calculated as analyte signal in the first blank droplet immediately following a sample (analyte containing) droplet divided by the analyte signal in the sample droplet.

To modify a fused silica capillary with fluorinated silanes, the capillary was first rinsed with 10 volume equivalents of isopropyl alcohol. Then, the capillary was rinsed with 2% (v/v) trichloro(1*H*,1*H*,2*H*,2*H*-perfluorooctyl)silane in perfluorodecalin (PFD) by infusing this solution at a flow rate of 1 μL min^{-1} for 400 min. After the infusion was complete, the solution was left to sit for another 48 hours. Then, the capillary was rinsed with 20/80 MeOH/18 MΩ water containing 0.1% formic acid at a flow rate of 40 μL min^{-1} for 10 min. The capillary was used immediately after completing this protocol. Capillary was 250 μm i.d. × 360 μm o.d. by 70 cm long.

3. Results and discussion

3.1. Control of flow rate

An Agilent CE-MS source, a type of sheath-flow ESI source (Fig. 1), was used to create and infuse droplets using the Venturi effect. In the source, sample flows through a central channel that is coaxial with flows of sheath liquid and nebulizing gas (N_2). The Venturi effect in this system can be attributed to the constriction of nebulizing gas at the end of the MS source. The decrease in pressure at the end of the source creates a differential that is sufficient to aspirate liquid through the tubing threaded through the source. In this way, flow can be achieved without external pumps or valves. In preliminary experiments, flow could be established regardless of whether the sheath liquid was flowing or not, so long as the nebulizing pressure was sufficiently high (Fig. S2A). In contrast, sample flow could not be achieved while only the sheath liquid was flowing (Fig. S2B). These results demonstrate that the nebulizing gas is critical to the establishment of Venturi-induced flow.

We investigated the effect of capillary inner diameter, nebulizing pressure, and sample phase composition on Venturi-induced flow and droplet signal (Fig. 2 and Table 1). For studying droplet-MS signal, we used droplets composed of 2 μM butyl glufosinate (target analyte of screen), 2 μM acetylcholine, and 2 μM glufosinate in 20/80 MeOH/water containing 1% blue food dye. Glufosinate was tested as an internal standard due to its structural similarity to butyl glufosinate but ultimately not used due to its markedly lower MS response (*i.e.*, butyl glufosinate/glufosinate signal = 20). As such, butyl glufosinate signal was divided by acetylcholine signal to compare MS results across different experimental conditions. Measurements of flow rate under these conditions largely conformed to expectations. Increasing the capillary inner diameter

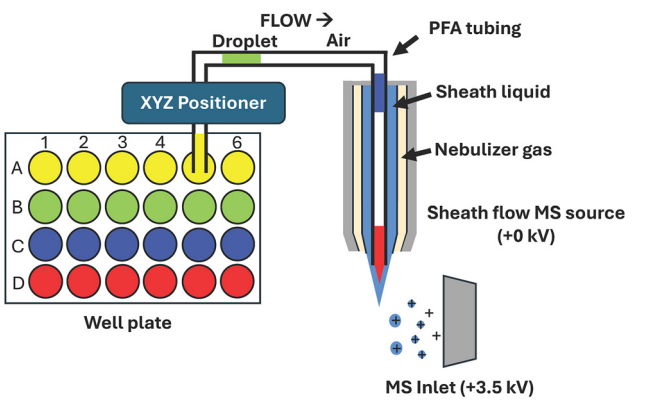

Fig. 1 Illustration of Venturi droplet-MS/MS method. Droplets segmented by air are generated from a well plate and flow directly into the mass spectrometer for analysis using the sheath-flow MS source. Tubing inlet is moved from well-to-well using an *x,y,z*-positioner. The Agilent sheath-flow MS source allows for threading of a 360 μm o.d. piece of tubing through the center of the source. A sheath liquid, illustrated in blue, and a nebulizing gas, illustrated in light orange, flow coaxially to the tubing. Illustration is not to scale.

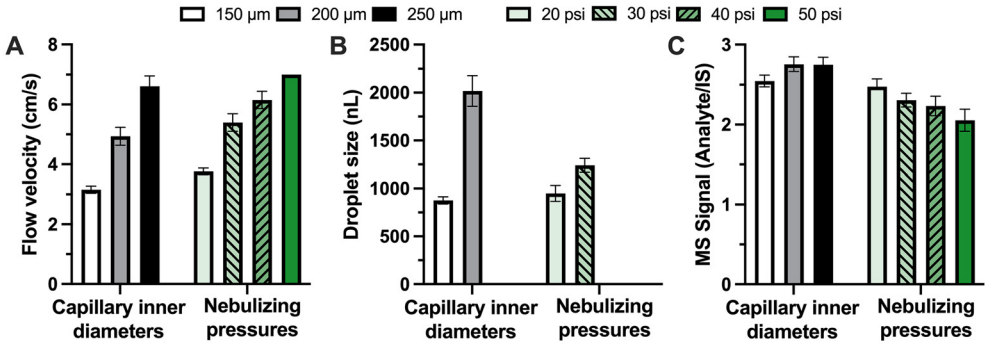

Fig. 2 Effect of transfer tubing inner diameter and nebulizing gas pressure on (A) flow velocity, (B) droplet size, and (C) resulting MS/MS signal of droplets generated and infused using Venturi effect. *Y* axis in (C) is butyl glufosinate divided by acetylcholine signal. Droplets contained 2 µM butyl glufosinate and acetylcholine in 20/80 MeOH/water containing 0.1% formic acid. Flow velocity values are plotted as average of n = 5 droplets, volumes are average of n = 10, and MS signals are average of n = 25. Error bars represent ± 1 SD. One droplet was in tubing at a time. Droplet size data was not collected for capillary i.d. = 250 µm, nebulizing pressure = 40 psi, and nebulizing pressure = 50 psi because droplets were longer than width of the camera frame (10 cm) used to measure droplet size. Fused silica capillary (70 cm long) was used to generate and infuse droplets.

Table 1 Droplet size and flow rate as a function of droplet composition (n = 6 droplets) using sheath liquid (20/80 MeOH/water containing 0.1% formic acid) flow rate = 0.1 mL min^{-1} and nebulizing pressure = 60 psi. PFA tubing (150 µm i.d. × 70 cm long) was used to generate and infuse droplets

Droplet composition	Average droplet size (nL)	Average flow rate (µL min^{-1})
10% formic acid in water	976 ± 11	159 ± 6
Water	940 ± 26	163 ± 4
100 mM HEPES (reaction matrix)	778 ± 18	149 ± 3
Quenched reaction matrix	818 ± 30	138 ± 8
Diluted quenched reaction matrix	842 ± 20	141 ± 3
50/50 MeOH/water	825 ± 25	128 ± 4
MeOH	1213 ± 22	216 ± 4

from 150 to 200 to 250 µm led to an increase in flow velocity and droplet size due to lower fluid resistance, with no significant effect on MS signal of the droplets (Fig. 2). Increasing the nebulizing pressure, which increases the pressure gradient,[32] resulted in greater Venturi-induced flow velocities and droplets sizes (Fig. 2A and B). This result is in agreement with a previous study on Venturi-induced flow in an ESI system.[32] A ~20% decrease in MS signal was observed when going from 20 to 50 psi (Fig. 2C). This is likely because the ESI conditions at 50 psi are not ideal for analyte ionization. These results indicate a compromise between sensitivity and flow velocity is required. Based on these trends, *i.e.*, an increase in velocity with a decrease in signal as nebulizer pressure increased, we elected to use the maximal nebulizing pressure available (60 psi) for screening, as analyte concentrations were expected to be high enough that sensitivity would not be limiting. This condition proved satisfactory for screens.

Sample composition affects Venturi-induced flow rate as well (Table 1). Lower viscosity samples (*e.g.*, methanol)[45,46] had larger droplet sizes and flow rates than those with higher viscosity (*e.g.*, water), as expected for Poiseuille flow. Based on pilot experiments, a sample composition of 20/80 MeOH/water containing 0.1% formic acid (v/v) was chosen for screening. Air was chosen as the segmenting phase since it has a lower viscosity compared to the perfluorinated oils that are normally used to segment droplets in microfluidics. Indeed, an earlier report asserted that a perfluorinated liquid decreased throughput of a Venturi droplet method.[38]

Positioning of the droplet tubing within the sheath-flow source can also affect the observed flow rate and therefore the resulting throughput of the method. For these experiments, the tubing exit was normally positioned 0.1 mm beyond the tip of the source. If the PFA tubing is extended 0.5 mm beyond the typical placement, flow is briefly observed before it comes to a stop (Fig. S3). Lack of stable flow is likely because the tubing is no longer in an area where the suction force created by the Venturi effect is powerful enough to sustainably aspirate liquid.

Other parameters were investigated that did not affect or only moderately affected the Venturi-induced flow rate including: capillary length (54, 70, 90 cm) and sheath flow rate (0.0, 0.1, and 0.2 mL min^{-1}). Decreasing transfer line length has been shown to affect Venturi-induced flow rate at short lengths (<50 cm),[32] but we did not observe any effect over 54 to 90 cm when generating and infusing ~800 nL plugs (Fig. S4). Decreasing the sheath liquid flow rate from 0.2 to 0.1 to 0.0 mL min^{-1} led to a slight decrease in Venturi-induced flow velocity, from 4.2 ± 0.1 cm s^{-1} to 3.8 ± 0.1 cm s^{-1} to 3.4 ± 0.1 cm s^{-1}, respectively (Fig. S4). The sheath flow was maintained at 0.1 mL min^{-1} for analysis of samples to aid in ionization of the analytes,[10] as well as to perform online dilution of the samples.

3.2. Multi-droplet flow

The above experiments were conducted so that only one droplet was in the tubing at a time. At the highest observed flow rate of 200 µL min^{-1} with a 250 µm i.d. × 70 cm long capillary, 20 s was required to clear a droplet from the capillary, thus limiting throughput to 0.05 samples per s. Closer

spacing of droplets would allow higher throughput but also require multiple droplets in the tubing at one time. Because the Venturi system is a constant pressure system, rather than constant flow, the number and volume of droplets in the capillary will influence the Venturi-induced flow rate. In particular, it has been shown that pressure drop is linearly proportional to the plug length and that small plugs (*i.e.*, dimensionless plug length <30) will have a larger plug resistance coefficient (C_f) than longer plugs (*i.e.*, dimensionless plug length >30).[47,48] We therefore investigated the potential for flowing multiple droplets stably through the transfer line.

Fig. 3 shows how flow rate and droplet signal change as a sequence of droplets are analyzed with multiple droplets present at once in the capillary. A set of 25 droplets was infused such that a droplet was introduced to the capillary every 2.6 s using a constant dwell time in sample (0.2 s) and air (2 s). At the beginning of the experiment, the capillary is filled with air, which has less fluidic resistance than the droplet solution. As such, the flow rate during droplet formation is high and the resulting droplet is the longest (270 dimensionless length) of the experiment. The second droplet is introduced while the first droplet is still in the capillary. As a result, the flow rate decreases to 94 μL min^{-1} and the second droplet is shorter with 210 dimensionless length. (Flow rates reported here represent the flow rate observed over ~6 cm of tubing at the halfway point between well plate inlet and mass spectrometer outlet.) The spacing detected between the droplets (as indicated by spacing in the MS trace) is at its highest because of the relatively high flow rates during formation *i.e.*, the droplets move quickly down the tube before the next droplet is formed. Droplet size, flow rate, and gap between droplets continue to decrease as more droplets are loaded into the capillary and fluidic resistance correspondingly increases (region 1 of Fig. 3). Eventually a stable period is achieved (region 2 of Fig. 3) with a stable flow rate (82.8 ± 3.4 μL min^{-1}), stable droplet length (102 ± 12 dimensionless length), and even spacing between droplets in the MS trace. During this time, ~9 droplets are in the capillary, and they are entering the mass spectrometer every 1.7 s. At the end of the sequence, droplets are no longer being loaded into the capillary. In this phase the capillary begins to fill with air, and the flow rate increases as fluidic resistance gradually decreases. As such, the droplets flow out of the capillary in narrow pulses and close together (region 3 of Fig. 3). The droplets detected in region 3 of Fig. 3 were formed using flow rates observed in region 2, so only the infusion flow rate, and not droplet nor spacing length, is affected by the increased flow rate observed in region 3. These results show that a stable period can be reached once nine droplets are present in the capillary under these conditions. Given these observations, two sets of 9 droplets were used to bookend the sample droplet sequence so that samples would be formed and sprayed under a constant flow condition.

The consistency observed in region 2 is not guaranteed when using the Venturi effect for multi-droplet flow and likely occurs in this case because the number of droplets in the capillary at any given moment is high enough that a relatively small (<15%) change in segmented fluid volume occurs when a droplet exits the capillary. With 9 droplets of equal volume in the capillary at a time, each has a relatively small effect (11% change) on total volume of segmented liquid in the capillary so that when one droplet exits the flow rate change is not large and stable flows are maintained.

Changing the space between droplets also affected the flow rate. Fig. 4 shows the effects of altering the time spent in the segmenting phase from 2 s (Fig. 4A and B) to 1 s (Fig. 4C and D) to 0.5 s (Fig. 4E and F). At 2 s spacing, oscillations in flow rate and droplet length in the middle of infusion (*i.e.*, from

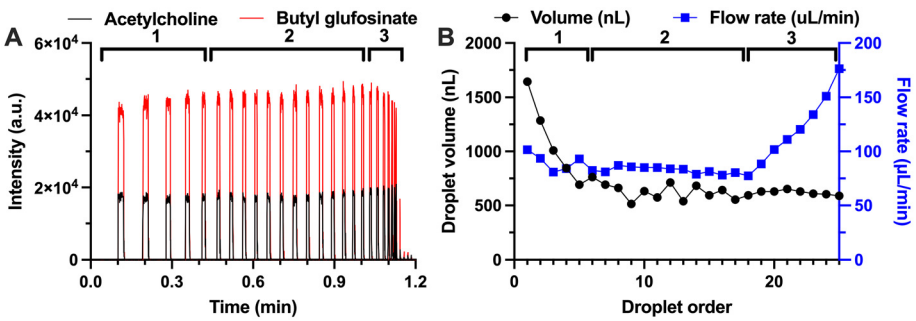

Fig. 3 Effect of tube filling with droplets on ESI-MS/MS signal for Venturi-generated samples. Droplets contained 3.3 μM butyl glufosinate, 2.5 μM acetylcholine, and 1% blue food dye in diluted reaction matrix. (A) MS/MS trace of droplets generated and infused using Venturi effect. The red trace represents acetylcholine and the black trace represents butyl glufosinate. The plot is divided into three regions, referred to as 1, 2, and 3, to represent different flow rate regimes observed while using the Venturi effect to drive flow. Region 1 occurs at start of droplet generation with the tubing empty. Region 1 is characterized by large initial droplet length that decreases as droplets enter the tube. Region 2 occurs when tubing is filled with droplets and is characterized by stable (<12% RSD) droplet lengths and flow rates. Region 3 occurs when droplets are no longer being introduced to the tubing and the tubing is being emptied. Region 3 has the same droplet lengths observed in region 2 but increasing flow rates as fluidic resistance decreases. (B) Dimensionless droplet lengths (black trace) and flow rates (blue trace) of the droplets generated and infused during the droplet-MS/MS trace in (A). The three regions (1, 2, and 3) in (B) correspond to the same regions and droplets in (A). Droplet spacing is >1000 nL in all cases. The *x* axis represents droplet order, meaning that an *x* value equal to ten corresponds to the tenth droplet that was generated and infused, *etc.* Nebulizing pressure = 20 psi. Fused silica capillary (250 μm i.d. × 70 cm long) was used to generate and infuse droplets.

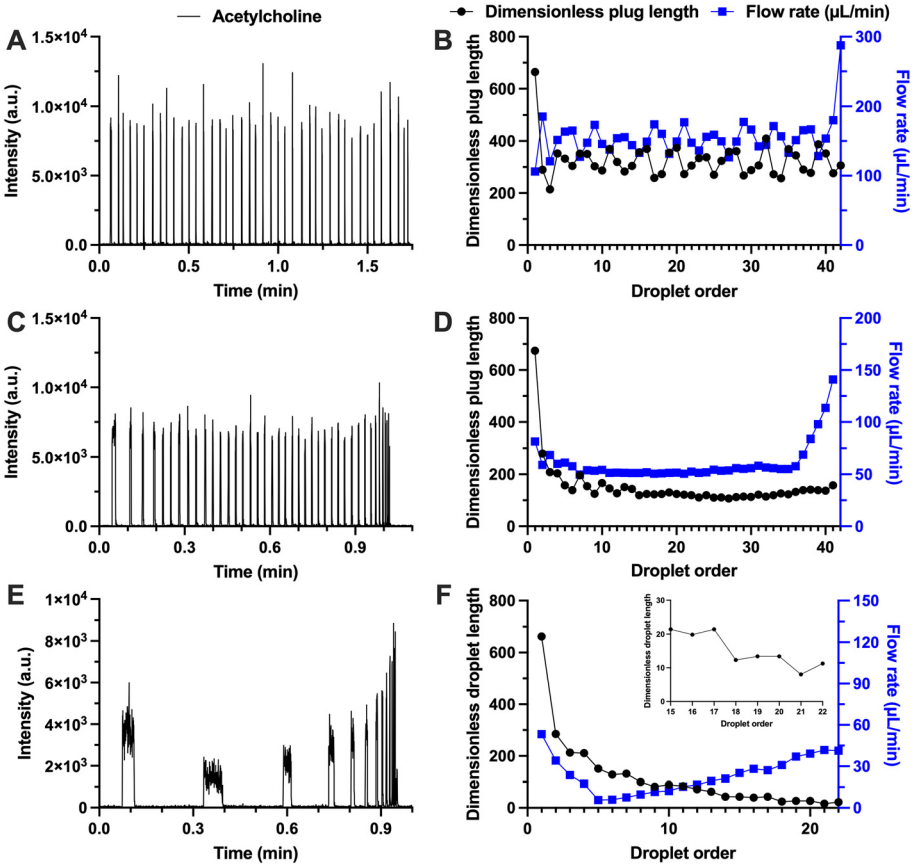

Fig. 4 MS/MS traces, dimensionless droplet lengths, and flow rates of droplets generated and infused using Venturi effect at the following dwell times in the segmenting phase: (A, B) 2 s (2–3 droplets in tubing at a time), (C, D) 1 s (9 droplets in tubing at a time), and (E, F) 0.5 s. Droplets contained 2.7 μM acetylcholine and 5% blue food dye in 20/80 MeOH/water containing 0.1% formic acid. (A, C, E) Droplet-MS/MS traces. (B, D, F) Dimensionless droplet lengths (black trace) and flow rates (blue trace). A total of 14 wells were sampled in triplicate, yielding an expected 42 droplets per run. Nebulizing pressure = 60 psi. PFA tubing (150 μm i.d. × 70 cm long) was used to generate and infuse droplets.

droplets 4 to 39) were observed (Fig. 4B). At this spacing, only 2–3 droplets were in the tubing at a given time, meaning that a 33% change in segmented liquid volume occurs if a droplet does not exit the tubing at the same time another is introduced. As a result, relatively large fluctuations in flow rate and droplet length were observed. In contrast, at 1 s gaps (Fig. 4C and D), 9 droplets were present yielding the same stable result as Fig. 3. With 0.5 s gaps (Fig. 4E and F), neither stable flow nor length was observed. Further, only 23 of 42 attempted droplet formations were detected. Likely, the droplet signals in Fig. 4E are inconsistent in terms of both signal maxima and width because of the changes in flow rate shown in Fig. 4F. Even smaller gaps (0.2 s) resulted in smaller droplets and subsequent flow stoppage (Table S1). This result is rationalized based on the finding that small droplets can require greater pressure than longer droplets to maintain a given flow rate; it has previously been demonstrated that a rapid, nonlinear increase in the plug resistance coefficient (C_f) is observed with biphasic air/water plug flow systems when the dimensionless plug length (L) is <30 as $L \rightarrow 0$.[47,48] The pressure drop associated with these plugs is linearly dependent on C_f, so a higher pressure drop will be required for systems possessing larger C_f values. Therefore, if enough droplets with $L < 30$ are introduced to a capillary, the pressure required for flow will become greater than what can be generated by the Venturi effect and flow will stop.

Taken together, these results show that the Venturi effect can be used to create a consistent flow; however, the effect is limited by the effects of friction of multiple droplets within the capillary. Based on these experiments, we used 380 nL droplet size and 330 μL min^{-1} flow rate for all screening experiments.

3.3. Figures of merit

Low carryover or cross-talk between adjacent samples is important to enable relative quantification. We evaluated carryover in PFA, fused silica, and fused silica with inner surface modified by 2% trichloro(1*H*,1*H*,2*H*,2*H*-perfluorooctyl)silane[40] transfer tubing (Fig. 5). Although PFA tubing was expected to have the lowest carryover, fused silica was of interest because it is available in larger i.d., potentially allowing higher flow rate and throughput. For carryover evaluation, fused silica

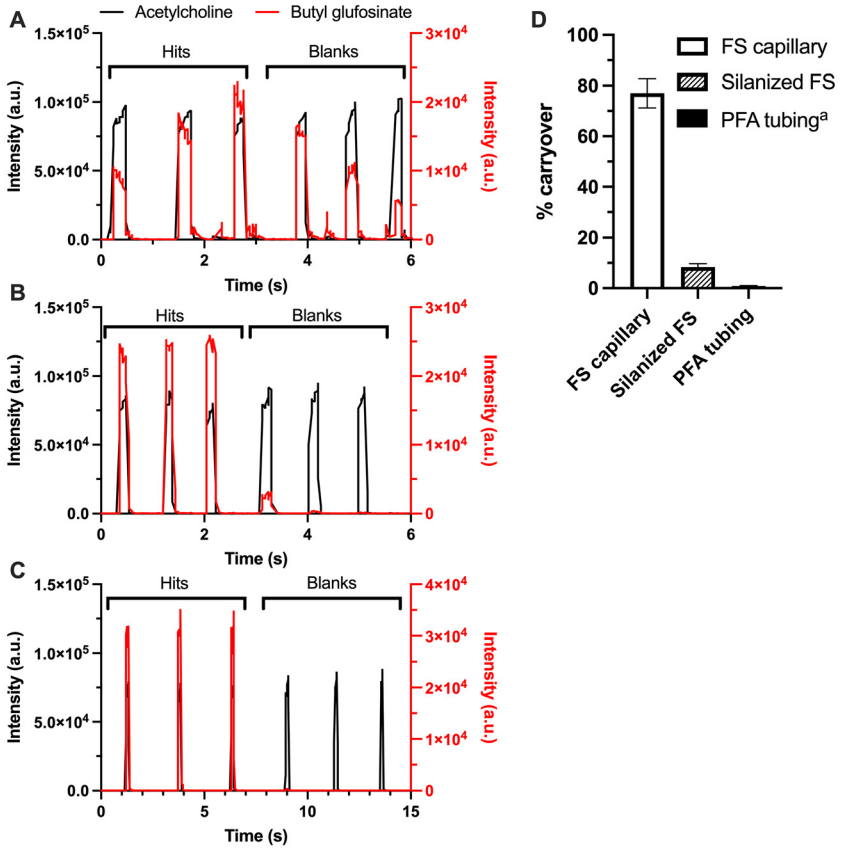

Fig. 5 Carryover of butyl glufosinate observed in fused silica capillary (FS capillary), fused silica that was treated with 2% silane in PFD (silanized FS), and PFA tubing. (A) Droplet-MS/MS trace of hit droplets (containing 3.3 μM butyl glufosinate and 2.5 μM acetylcholine in diluted reaction matrix) and blank droplets (containing 2.5 μM acetylcholine in diluted reaction matrix) generated and infused using Venturi effect with FS capillary. Droplets were 1210 ± 56 nL and flowed at 454 ± 7 μL min^{-1}. (B) Droplet-MS/MS trace of hit and blank droplets generated and infused using Venturi effect with silanized FS. Droplets were 1190 ± 130 nL and flowed at 578 ± 4 μL min^{-1}. (C) Droplet-MS/MS trace of hit and blank droplets generated and infused using Venturi effect with PFA tubing. Droplets were 344 ± 25 nL and flowed at 168 ± 11 μL min^{-1}. In (A), (B), and (C), the black trace represents acetylcholine, and its intensity is plotted on the left *y*-axis. The red trace represents butyl glufosinate, and its intensity is plotted on the right *y*-axis. (D) Percent carryover observed with FS capillary, silanized FS, and PFA tubing. Bars are plotted as average of n = 12 droplets and error bars represent ± 1 SD. Nebulizing pressure = 60 psi. [a] PFA tubing had an inner diameter = 150 μm and droplet analysis throughput = 0.5 samples per s, while FS capillaries had inner diameters = 250 μm and droplet analysis throughput = 1 sample per s. Other dimensions (360 μm o.d. × 70 cm long) were the same.

capillaries were 250 μm i.d. and PFA tubing was 150 μm i.d. All capillaries/tubing had 360 μm o.d. and were 70 cm long. Modifying the fused silica surface led to a decrease in butyl glufosinate carryover from 77 ± 6% to 8.4 ± 1.3% in the first blank droplet infused immediately after a droplet containing the analyte. The PFA tubing offered the lowest carryover at 0.88 ± 0.16% (Fig. 5). This low carryover may be due to the surface chemistry and the lower rate of infusion[40] (0.5 samples per s compared to 1 sample per s with fused silica) caused by its smaller inner diameter. PFA tubing was selected moving forward despite it offering a lower flow rate compared to capillaries with larger inner diameters, as it was anticipated that the lower carryover would make quantification easier and more accurate.

The detection limit for butyl glufosinate was 0.5 μM, as determined by the limit of the blank method,[49] measured in 381 ± 24 nL droplets composed of diluted reaction matrix flowing at 329 ± 70 μL min^{-1}. Calibrations were linear between 0.7 to 3.3 μM butyl glufosinate (Fig. S5), which is the expected range of concentrations in the samples. Signal was consistent (7% RSD) across a mock screen of wells (n = 96) containing 3.3 μM butyl glufosinate standard in the screening matrix (Fig. S6).

3.4. Evaluating hydantoinase activity with high-throughput screening

The method was tested on hydantoinase variants developed during a directed evolution campaign to generate a biocatalytic route to enantioselective production of L-butyl glufosinate. The engineering goal was to increase L-selectivity of the hydantoinase for more efficient L-butyl glufosinate production, and Scheme 1 shows the dual enzyme strategy used for the reaction. In this scheme, a hydantoinase that shows D-selectivity acts on a racemic mixture of hydantoin butyl glufosinate to

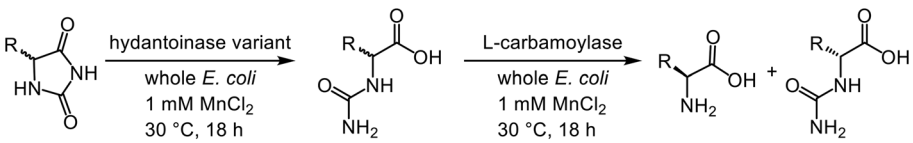

Scheme 1 Use of the hydantoinase process to selectively produce L-amino acids. As both enzymes retain stereochemistry at the α-carbon, the enantioselectivity of the hydantoinase is important in determining the overall conversion of hydantoin to L-amino acid.

produce both D- and L-carbamoylic acid butyl glufosinate. The L-carbamoylic acid is then converted by an L-selective carbamoylase to produce the final L-butyl glufosinate product. Therefore, any increase in butyl glufosinate detected in screening is assumed to be L-butyl glufosinate and is attributed to an increase in L-carbamoylic acid production by the hydantoinase. L-Selectivity is defined as butyl glufosinate peak area divided by the sum of carbamoylic acid and butyl glufosinate peak areas determined by achiral LC-MS. Selected enzyme reactions (n = 36) were validated with chiral LC-MS to verify that ≥99% L-butyl glufosinate was produced and ≥81% D-carbamoylic acid (area % of enantiomer divided by L- and D-enantiomers) remained.

Fig. 6A shows an MS trace for screening 96 variants in triplicate. A total of 369 droplets were infused over 15 min. The experiment included calibration standards and marker droplets, containing a higher concentration of acetylcholine than samples, to ensure sample registry with wells. (Another 9 droplets were infused at either end for stable flow as described above). Droplets were 381 ± 24 nL and flowed at 329 ± 70 μL min^{-1}. To test the accuracy of the method, fold improvement of butyl glufosinate production by the enzyme variants relative to template enzyme (*i.e.*, starting enzyme that was modified) was compared to that determined by achiral LC-MS (Fig. 6B) showing good agreement. Extending the analysis to a total of 283 enzyme reactions from 3 separate 96-well plate screens, a high correlation between the droplet-MS and achiral LC-MS methods is observed (R^2 = 0.9185) (Fig. 6C). This result indicates that the Venturi method provides comparable results to LC-MS but is 67-fold faster (0.4 samples per s droplet infusion rate compared to 0.006 samples per s analysis rate of 3 min achiral LC-MS method). Additionally, four enzyme variants from the plate shown in Fig. 6A were also screened by chiral LC-MS and were confirmed as having increased L-selectivity, with the top performing variant that was also identified as a hit by droplet-MS showing an increase from 20 to 25% L-selectivity. As such, it is thought that this method could be useful for performing enzyme engineering *via* directed evol-

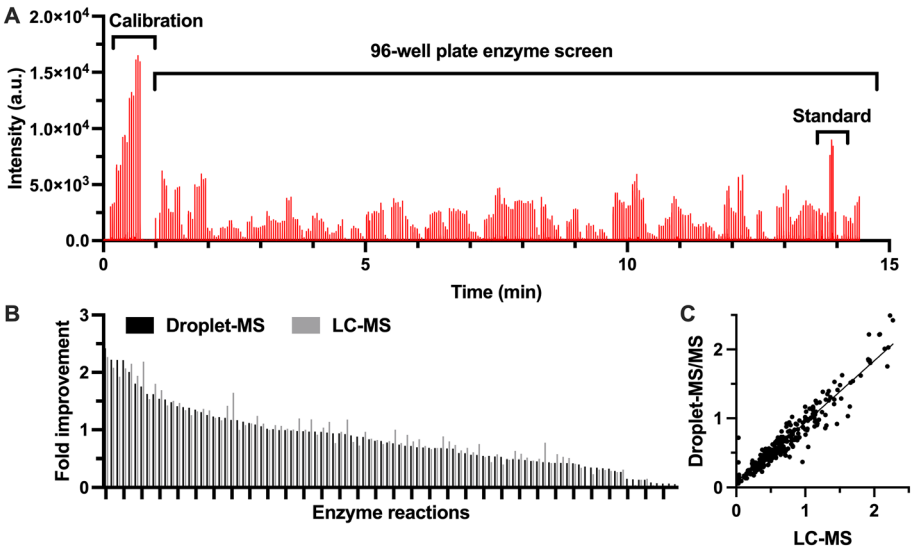

Fig. 6 Enzyme variant screen with Venturi droplet-MS/MS. (A) MS/MS signal trace of calibration standards and 96-well plate of enzyme variant reactions producing butyl glufosinate. The red trace represents butyl glufosinate. The trace for acetylcholine, which was used to mark droplets, is not shown for better viewing of the butyl glufosinate trace. Droplets were 381 ± 24 nL and flowed at 329 ± 70 μL min^{-1}. (B) Fold improvement values obtained for a 96-well plate of enzyme variants analyzed in (A), which corresponds to 84 variants and 12 control reactions. Data is arranged in descending order of droplet-MS fold improvement values. The x-axis represents all enzyme variant reactions in a 96-well plate, and the fold improvement values determined by droplet-MS (black bar) and achiral LC-MS (gray bar) are plotted side by side for a given x position, which represents a single enzyme variant reaction. (C) Plot of droplet-MS *vs.* achiral LC-MS fold improvement and resulting regression for 283 enzyme reaction samples. The equation describing the regression line is y = 0.90x + 0.04 with R^2 = 0.9185. Nebulizing pressure = 60 psi. PFA tubing (150 μm i.d. × 70 cm long) was used to generate and infuse droplets.

ution, since it may reduce time associated with analyzing thousands of enzyme variants.

3.5. Further improvements

Droplet sample introduction is a simple way to achieve high-throughput MS analysis with low sample consumption. The use of the Venturi effect for generating flow facilitates operation by combining droplet generation and infusion steps. Nevertheless, there are some limitations that may be addressed. If samples were not sufficiently filtered, then debris buildup in the tubing resulted in inconsistent flow. Given that filtering and other sample preparation steps can be performed in batches at high throughput, this would not be a limitation in many cases. Alternatively, rinse protocols may be developed at the expense of some throughput. The throughput was limited by the ability of the Venturi effect generated within this source to overcome flow resistance of multiple small droplets. Higher flows may be possible with a custom source or larger i.d. tubing, which would allow for higher throughput.

4. Conclusion

We show a high-throughput, well plate-based droplet-ESI-MS method with an automated droplet generation to infusion component. Up to 0.4 samples per s analysis was achieved with this system. The setup is simple as it only requires a well plate, an *x*,*y*,*z*-positioner, tubing, and an MS source capable of creating the Venturi effect. This work builds upon V-EASI (0.6 samples per s),[38] OPI-MS (0.5[35] to 3[31,32] samples per s),[31,32,35] and RAVE MS work (0.1 samples per s)[42] by demonstrating similar or higher throughput without the requirement of specialty equipment (*i.e.* custom source[31,38] or open port interface[31,32,35]). Additionally, we detail important variables for changing the throughput of the Venturi droplet-MS method, such as droplet tubing inner diameter, nebulizing pressure, sample phase composition, and droplet size. The system was demonstrated by screening enzyme variants but should be applicable to other high-throughput MS applications from multi-well plates.

Author contributions

Bridget E. Murray: conceptualization, formal analysis, investigation, methodology, validation, visualization, writing – original draft, writing – reviewing & editing. Roger C. Diehl: conceptualization, formal analysis, investigation, methodology, writing – reviewing and editing. Moritz Pott: conceptualization, methodology, funding acquisition, project administration, resources, supervision, writing – reviewing & editing. Daniel Holland-Moritz: conceptualization, writing – reviewing & editing. Alison R. H. Narayan: conceptualization, funding acquisition, project administration, resources, supervision, writing – reviewing & editing. Robert T. Kennedy: conceptualization, funding acquisition, project administration, resources, supervision, writing – reviewing & editing.

Conflicts of interest

There are no conflicts to declare.

Data availability

Full data sets are available upon reasonable request to the corresponding author.

Supplementary information (SI) is available. LC-MS trace of enzyme reaction, effect of nebulizing gas and sheath flow rate on method, effect of tubing placement on method, effect of capillary length and sheath flow rate on method, calibration curve data, mock 96-well plate screen, and dimensionless plug lengths for condition where flow stopped. See DOI: https://doi.org/10.1039/d6an00065g.

Acknowledgements

The research was supported by a grant from BASF (A. R. H. N. and R. T. K.) and NIH RO1 014513 (R. T. K.). The authors acknowledge G. Thomas Knecht for helpful discussions.

References

1 C. S. Shultz and S. W. Krska, *Acc. Chem. Res.*, 2007, **40**, 1320–1326.
2 T. R. Covey, in *High–Throughput Mass Spectrometry in Drug Discovery*, 2023, pp. 1–74. DOI: 10.1002/9781119678496.ch1.
3 S. W. Krska, D. A. DiRocco, S. D. Dreher and M. Shevlin, *Acc. Chem. Res.*, 2017, **50**, 2976–2985.
4 L. E. Zetzsche, J. A. Yazarians, S. Chakrabarty, M. E. Hinze, L. A. M. Murray, A. L. Lukowski, L. A. Joyce and A. R. H. Narayan, *Nature*, 2022, **603**, 79–85.
5 W. Z. Shou and J. Zhang, *Expert Opin. Drug Metab. Toxicol.*, 2010, **6**, 321–336.
6 W. Z. Shou, *J. Pharm. Anal.*, 2020, **10**, 201–208.
7 R. Grainger and S. Whibley, *Org. Process Res. Dev.*, 2021, **25**, 354–364.
8 Y. Xin, S. W. Foster, D. M. Makey, D. Parker, J. Bradow, X. Wang, S. Berritt, R. Mongillo, J. P. Grinias and R. T. Kennedy, *Anal. Chem.*, 2024, **96**, 4693–4701.
9 R. A. Shepherd, C. A. Fihn, A. J. Tabag, S. M. K. McKinnie and L. M. Sanchez, *Nat. Prod. Rep.*, 2025, **42**, 1037–1054.
10 X. W. Diefenbach, I. Farasat, E. D. Guetschow, C. J. Welch, R. T. Kennedy, S. Sun and J. C. Moore, *ACS Omega*, 2018, **3**, 1498–1508.
11 B. Liu, S. Li and J. Hu, *Am. J. PharmacoGenomics*, 2004, **4**, 263–276.

12 S. Akagi, C. Nakajima, Y. Tanaka and Y. Kurihara, *J. Biosci. Bioeng.*, 2018, **125**, 464–469.
13 F. Pu, N. L. Elsen and J. D. Williams, *ACS Med. Chem. Lett.*, 2020, **11**, 2108–2113.
14 F. Gielen, R. Hours, S. Emond, M. Fischlechner, U. Schell and F. Hollfelder, *Proc. Natl. Acad. Sci. U. S. A.*, 2016, **113**, E7383–E7389.
15 J. J. Agresti, E. Antipov, A. R. Abate, K. Ahn, A. C. Rowat, J. C. Baret, M. Marquez, A. M. Klibanov, A. D. Griffiths and D. A. Weitz, *Proc. Natl. Acad. Sci. U. S. A.*, 2010, **107**, 4004–4009.
16 F. W. McLafferty, *Science*, 1981, **214**, 280–287.
17 B. E. Murray, L. I. Penabad and R. T. Kennedy, *Curr. Opin. Biotechnol.*, 2023, **82**, 102962.
18 D. J. Steyer and R. T. Kennedy, *Anal. Chem.*, 2019, **91**, 6645–6651.
19 D. A. Holland-Moritz, M. K. Wismer, B. F. Mann, I. Farasat, P. Devine, E. D. Guetschow, I. Mangion, C. J. Welch, J. C. Moore, S. Sun and R. T. Kennedy, *Angew. Chem., Int. Ed.*, 2020, **59**, 4470–4477.
20 K. Wink, M. van der Loh, N. Hartner, M. Polack, C. Dusny, A. Schmid and D. Belder, *Angew. Chem., Int. Ed.*, 2022, **61**, e202204098.
21 D. A. Pereira and J. A. Williams, *Br. J. Pharmacol.*, 2007, **152**, 53–61.
22 M. J. Wildey, A. Haunso, M. Tudor, M. Webb and J. H. Connick, in *Platform Technologies in Drug Discovery and Validation*, ed. R. A. Goodnow, Academic Press, 2017, vol. 50, pp. 149–195.
23 J. J. Douglas, A. D. Campbell, D. Buttar, G. Fairley, M. J. Johansson, A. C. McIntyre, A. J. Metrano, R. S. Morales, R. H. Munday, T. V. Q. Nguyen, S. Staniland, M. Tavanti, E. Weis, S. D. Yates and Z. Zhang, *ACS Catal.*, 2025, **15**, 5229–5256.
24 J. R. Neifeld, L. E. Regester, J. M. Holler, S. P. Vorce, J. Magluilo Jr., G. Ramos and T. Z. Bosy, *J. Anal. Toxicol.*, 2016, **40**, 379–387.
25 D. Tao, M. Xu, A. Farkhondeh, A. P. Burns, S. Rodems, M. Might, W. Zheng and C. A. LeClair, *Talanta*, 2021, **231**, 122384.
26 M. Rohman and J. Wingfield, in *High Throughput Screening: Methods and Protocols*, ed. W. P. Janzen, Springer New York, New York, NY, 2016, pp. 47–63. DOI: 10.1007/978-1-4939-3673-1_3.
27 T. Bretschneider, C. Ozbal, M. Holstein, M. Winter, F. H. Buettner, S. Thamm, D. Bischoff and A. H. Luippold, *SLAS Technol.*, 2019, **24**, 386–393.
28 I. Sinclair, R. Stearns, S. Pringle, J. Wingfield, S. Datwani, E. Hall, L. Ghislain, L. Majlof and M. Bachman, *J. Lab. Autom.*, 2016, **21**, 19–26.
29 I. Sinclair, M. Bachman, D. Addison, M. Rohman, D. C. Murray, G. Davies, E. Mouchet, M. E. Tonge, R. G. Stearns, L. Ghislain, S. S. Datwani, L. Majlof, E. Hall, G. R. Jones, E. Hoyes, J. Olechno, R. N. Ellson, P. E. Barran, S. D. Pringle, M. R. Morris and J. Wingfield, *Anal. Chem.*, 2019, **91**, 3790–3794.
30 M. J. Smith, D. P. Ivanov, R. J. M. Weber, J. Wingfield and M. R. Viant, *Anal. Chem.*, 2021, **93**, 9258–9266.
31 S. Guo, Z. Wen, L. Chen, M. Jia, Y. Wang and J. Sun, *Anal. Chem.*, 2025, **97**, 11496–11505.
32 T. T. Habe, C. Liu, T. R. Covey, R. P. Simon, W. Reindl, F. H. Buttner, M. Winter, D. Bischoff, A. H. Luippold and F. Runge, *Anal. Chem.*, 2020, **92**, 12242–12249.
33 C. Liu, G. J. Van Berkel, D. M. Cox and T. R. Covey, *Anal. Chem.*, 2020, **92**, 15818–15826.
34 C. Liu, G. J. Van Berkel, P. Kovarik, J. B. Perot, V. Inguva and T. R. Covey, *Anal. Chem.*, 2021, **93**, 8559–8567.
35 H. Zhang, C. Liu, W. Hua, L. P. Ghislain, J. Liu, L. Aschenbrenner, S. Noell, K. J. Dirico, L. F. Lanyon, C. M. Steppan, M. West, D. W. Arnold, T. R. Covey, S. S. Datwani and M. D. Troutman, *Anal. Chem.*, 2021, **93**, 10850–10861.
36 S. Sun, M. Hou, C. Lai, Q. Yang, J. Gao, X. Lu, X. Wang and Q. Yu, *Talanta*, 2024, **266**, 125008.
37 Y. Zhu, Q. Zhang, Q. Zhang, J. Lu, K. Wang, R. Zhang and Q. Yu, *Anal. Chem.*, 2022, **94**, 7417–7424.
38 N. Liu, Y. Liu, Y. Yang, L. He and J. Ouyang, *Anal. Chim. Acta*, 2016, **913**, 86–93.
39 C. I. D'Amico, D. A. Polasky, D. J. Steyer, B. T. Ruotolo and R. T. Kennedy, *Anal. Chem.*, 2022, **94**, 13084–13091.
40 S. Sun and R. T. Kennedy, *Anal. Chem.*, 2014, **86**, 9309–9314.
41 D. M. Makey, R. C. Diehl, Y. Xin, B. E. Murray, D. R. Stoll, B. T. Ruotolo, J. P. Grinias, A. R. H. Narayan, V. Lopez-Carillo, M. Stark, P. Johnen and R. T. Kennedy, *Anal. Chem.*, 2023, **95**, 17028–17036.
42 D. A. Holland-Moritz, S. R. Moor, J. B. Parry, E. J. Medcalf, C. M. Eberle, A. C. Strakham, S. T. Grosser, H. Hu, N. P. Dunham and M. Gantz, *React. Chem. Eng.*, 2025, **10**, 2243–2251.
43 Y. Mukohara, T. Ishikawa, K. Watabe and H. Nakamura, *Biosci., Biotechnol., Biochem.*, 1994, **58**, 1621–1626.
44 Z. Zhang, J. Richardson and B. Shah, *Anal. Biochem.*, 2023, **674**, 115211.
45 N. Weisbrod, Y. Yechieli, S. Shandalov and N. Lensky, *J. Hydrol.*, 2016, **532**, 46–51.
46 J. W. Thompson, T. J. Kaiser and J. W. Jorgenson, *J. Chromatogr. A*, 2006, **1134**, 201–209.
47 M. T. Kreutzer, F. Kapteijn, J. A. Moulijn, C. R. Kleijn and J. J. Heiszwolf, *AIChE J.*, 2005, **51**, 2428–2440.
48 Z. Che, T. N. Wong and N.-T. Nguyen, *Int. J. Heat Fluid Flow*, 2011, **32**, 1005–1013.
49 D. A. Armbruster and T. Pry, *Clin. Biochem. Rev.*, 2008, **29**(Suppl 1), S49–S52.